The high thermal stability of the synthetic zeolite K–L: Dehydration mechanism by in situ SR-XRPD experiments

Elsevier Editorial System(tm) for Microporous & Mesoporous Materials
Manuscript Draft

Manuscript Number: MICMAT-D-12-01231R1

Title: The high thermal stability of the synthetic zeolite K-L: dehydration mechanism by in-situ SR-XRPD experiments

Article Type: Full Length Article

Keywords: Zeolite K-L, dehydration mechanism, thermal behavior, in-situ synchrotron X-ray powder diffraction

Corresponding Author: Prof. Giovanna Vezzalini, Full Professor

Corresponding Author's Institution: University of Modena and Reggio Emilia

First Author: Giovanna Vezzalini

Order of Authors: Giovanna Vezzalini; Lara Gigli; Rossella Arletti; Simona Quartieri; Francesco Di Renzo

Abstract: Thermally induced structural modifications of a synthetic zeolite L [K8.46 (Al8.35 Si27.53) O72 *17.91H2O, framework type LTL, s.g. P6/mmm, a =18.3367(1) and c = 7.5176(1) Å] were studied by temperature-resolved synchrotron X-ray powder diffraction. In the investigated temperature range (RT-814°C), neither structure breakdown nor phase transitions occurred. The largest unit cell deformation was observed between 100º and 240°C, accompanied by an increase and decrease of the a and c cell parameters, respectively. After complete water release, an inversion of the a and c parameter behavior was observed, while the cell volume continued to increase, although following a more flattened curve. Overall, in the investigated T range, a small cell volume increase of 0.7% was observed. The release of the five water molecules present in zeolite L started with the most weakly bonded one and occurred between 80º and 240°C. During dehydration the framework underwent minor rearrangements, which facilitated water release: the apertures of the main 12-ring and the 8-ring channels became more circular and the 6-membered rings became more hexagonal. The thermal expansion of zeolite L, very unusual for a non-siliceous zeolite, was interpreted and compared with previous data reported in literature for this porous material, and with the behavior of the synthetic phases ITQ-4 and CIT-5.

Highlights

In-situ dehydration of zeolite L was studied between RT and 814 °C. > The largest unit cell deformation was observed in correspondence of water release. > In the investigated T range, a small cell volume increase of 0.7% was observed. > Water release is facilitated by minor framework deformations. >The thermal expansion of zeolite L is very unusual for a non-siliceous zeolite.

*Graphical Abstract (for review)

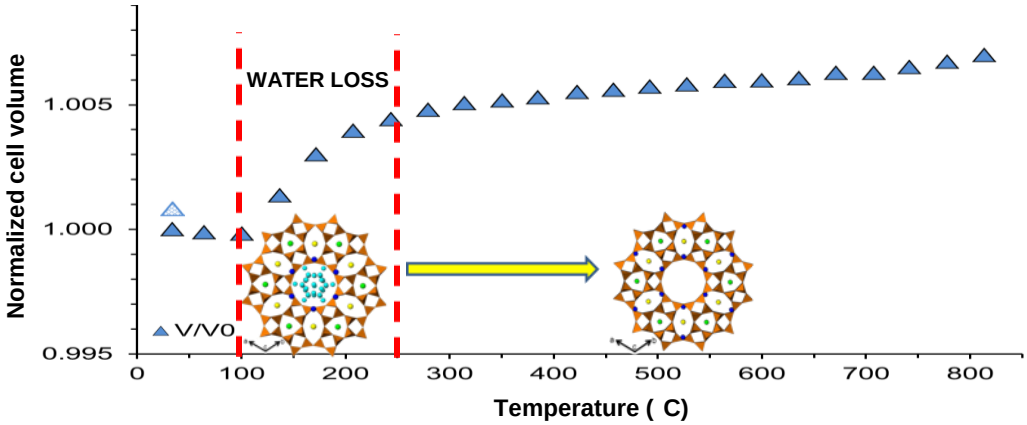

The high thermal stability of the synthetic zeolite K-L: dehydration mechanism by in-situ SR-XRPD experiments

Lara Gigli[1], Rossella Arletti[2], Simona Quartieri[3], Francesco Di Renzo[4], Giovanna Vezzalini[1*]

[1]Dipartimento di Scienze Chimiche e Geologiche, Università di Modena e Reggio Emilia, Via S. Eufemia 19, 41100 Modena, Italy.

[2]Dipartimento di Scienze della Terra, Università di Torino, Via Valperga Caluso 35, 10125 Torino, Italy

[3]Dipartimento di Fisica e di Scienze della Terra, Università di Messina, Viale Ferdinando Stagno d'Alcontres 31, 98166 Messina S. Agata, Italy.

[4]Institut Charles Gerhardt de Montpellier, UMR 5253 CNRS-UM2-ENSCM-UM1, 8 rue Ecole Normale, 34296 Montpellier, France.

Corresponding author:

Giovanna Vezzalini
Dipartimento di Scienze della Terra, Università di Modena e Reggio Emilia
Largo Sant' Eufemia, 19
I-41100 Modena, Italy.
Tel. +39-(0)59-2055827
Fax. +39-(0)59-2055887
e-mail mariagiovanna.vezzalini@unimore.it

Running Title: Dehydration mechanism of zeolite K-L

The high thermal stability of the synthetic zeolite K-L: dehydration mechanism by in-situ SR-XRPD experiments

Lara Gigli[1], Rossella Arletti[2], Simona Quartieri[3], Francesco Di Renzo[4], Giovanna Vezzalini[1*]

[1]Dipartimento di Scienze Chimiche e Geologiche, Università di Modena e Reggio Emilia, Via S. Eufemia 19, 41100 Modena, Italy.

[2]Dipartimento di Scienze della Terra, Università di Torino, Via Valperga Caluso 35, 10125 Torino, Italy

[3]Dipartimento di Fisica e di Scienze della Terra, Università di Messina, Viale Ferdinando Stagno d'Alcontres 31, 98166 Messina S. Agata, Italy.

[4]Institut Charles Gerhardt de Montpellier, UMR 5253 CNRS-UM2-ENSCM-UM1, 8 rue Ecole Normale, 34296 Montpellier, France.

ABSTRACT

Thermally induced structural modifications of a synthetic zeolite L [$K_{8.46}(Al_{8.35}Si_{27.53})O_{72} \cdot 17.91H_2O$, framework type LTL, s.g. *P6/mmm*, *a* =18.3367(1) and *c* = 7.5176(1) Å] were studied by temperature-resolved synchrotron X-ray powder diffraction. In the investigated temperature range (RT-814°C), neither structure breakdown nor phase transitions occurred. The largest unit cell deformation was observed between 100º and 240°C, accompanied by an increase and decrease of the *a* and *c* cell parameters, respectively. After complete water release, an inversion of the *a* and *c* parameter behavior

was observed, while the cell volume continued to increase, although following a more flattened curve. Overall, in the investigated T range, a small cell volume increase of 0.7% was observed. The release of the five water molecules present in zeolite L started with the most weakly bonded one and occurred between 80º and 240°C. During dehydration the framework underwent minor rearrangements, which facilitated water release: the apertures of the main 12-ring and the 8-ring channels became more circular and the 6-membered rings became more hexagonal. The thermal expansion of zeolite L, very unusual for a non-siliceous zeolite, was interpreted and compared with previous data reported in literature for this porous material, and with the behavior of the synthetic phases ITQ-4 and CIT-5.

Keywords: Zeolite K-L, dehydration mechanism, thermal behavior, in-situ synchrotron X-ray powder diffraction.

1. Introduction

The study of the dehydration processes of zeolites and of their consequent structural modifications is of particular importance, owing to the wide application of these materials as molecular sieves, sorbents, and catalysts. Specifically, the knowledge of temperature-induced structural modifications and the stability fields of these materials is of prime importance to assure their persistence and effectiveness in technological applications. Zeolite thermal behavior has been largely and systematically studied by many authors. In particular it has been schematized by Alberti and Vezzalini [1] and reviewed by Ståhl [2], Artioli [3], Bish and Carey [4] and Cruciani [5] and related literature.

Recent innovative applications of zeolites regard their use as host matrices for the supramolecular organization of a large variety of guests, and also as key components of a promising novel class of hybrid materials. The inclusion of guest molecules into ordered

one-dimensional channel systems is particularly intriguing, as the resulting host-guest compounds may exhibit peculiar new properties. These hybrid materials can be exploited in several research fields, as devices for solar energy harvesting, processing/storing of information, and advanced sensing technology for analytics and diagnostics on the nanoscale[6,7,8].

Synthetic zeolite L (ideal formula $K_6Na_3Al_9Si_{27}O_{72} \cdot 21H_2O$, framework type LTL [9], s.g. *P6/mmm*, unit cell dimensions *a* =18.40(4) Å and *c* = 7.52(3) Å)[10] (Figure 1a,b) configures itself as an ideal host matrix because its arrays of parallel channels impose severe space restrictions and geometrical constraints on any inserted guest species . As a result, very high concentrations of well oriented molecules can be obtained[6,7,8]. In view of the well-known affinity of zeolites for water, stability of the hybrid materials upon hydration is particularly critical. In fact, in many dye-zeolite composites exposed to air at room temperature (RT), as a consequence of the entrance of water molecules, a displacement of the organic dye from the channels is observed [11]. Upon heating, and hence drying, the guest molecules can be re-inserted.

In the framework of a wider project aimed at the study of the incorporation mechanism of organic molecules in zeolite L[12], a detailed knowledge of the dehydration mechanism and thermal stability of this zeolite is of fundamental importance.

Since its first synthesis in 1968 [13], the structures of zeolite LTL have been reported in various cationic forms, tetrahedral ion and hydration status, such as: hydrated (Na,K)-L[10], hydrated (K, Ba)-L [14], K- GaSi L[15], Rb-GaSi L[16], AlPO-LTL [17], LZ-212 [18] and the natural mineral perlialite [19].

The LTL framework [10] is built from columns of cancrinite cages stacked with double six membered rings (D6R) along the *c* axis. These columns are connected to form larger circular 12-ring (12MR) channels and smaller elliptical 8-ring (8MR) channels (which run along the *c* axis. The main channels are connected to the parallel 8-ring

channels by a non-planar boat-shaped 8MR. Four extraframework cationic sites were localized in sample BV[10] : i) site A - in the center of the D6R - is partially occupied by both K and Na and is coordinated to six framework oxygen atoms; ii) site B - in the center of the cancrinite cage - is fully occupied by K and is coordinated to six framework oxygen atoms; iii) site C - located in the center of the 8MR channel parallel to the *c* axis, midway between the centers of two adjacent cancrinite cages - is occupied by K (with an occupancy factor of 0.9) and is coordinated by four oxygen atoms; iv) site D - the only cation site found in the main 12MR channel - is partially occupied by Na and is coordinated to six oxygen atoms and two water molecules. The BV sample contains 21 water molecules, distributed over eight extraframework sites in the main channel . They are partially occupied and weakly bonded to the framework.

Lee et al. [16] determined that in the rubidium gallosilicate form, water molecules constitute a sequence of hydrogen bonded water clusters and cation-water layers running along *c*.

Newsam [20] reports the results of a neutron powder diffraction study – performed at 298 and 78 K - of an in-vacuum-dehydrated potassium zeolite L and of the same zeolite containing perdeuteriobenzene molecules. The average framework geometry exhibits only small changes as a consequence of dehydration or benzene sorption, suggesting that the LTL framework is rather inflexible. The same author refined the structure of the dehydrated gallium zeolite L [15] and underlined that the non-framework cation configuration is similar to that described for the aluminum zeolite L[10], suggesting that little change in cation distribution accompanies dehydration.

This work aims to analyze in detail the kinetics and mechanisms of zeolite L dehydration, by means of in-situ high temperature synchrotron X-ray powder diffraction (XRPD) experiments and complete structural refinements.

2. Experimental Methods

The zeolite L sample used in this work was synthesized as follows. A template solution A was prepared by dissolving 6 g KOH (SdS) and 3.15 g $Al(OH)_3$ (Merck) in 10 mL de-ionized water. The solution was boiled until clear, cooled to RT and restored to 10 mL volume by addition of water. A solution B was prepared by diluting 30 g Ludox HS-40 (Dupont) with 20 g H_2O. Then 3 mL of 0.01 molar $Mg(NO_3)_2$ solution, corresponding to a Mg/silica molar ratio 9300, were added to solution B in order to improve the selectivity of the synthesis [21]. Solutions A and B and a further 4 mL water were poured into a 130 mL stainless steel autoclave while stirring. The autoclave was sealed and heated at 150 °C for 96 h without stirring. After cooling to RT, the suspension was filtered, washed with water until pH 9, and dried at 80°C.

The chemical composition was determined using a Cameca SX 50 Electron microprobe on a pellet of the zeolite L (experimental conditions: 20 kV, beam current 2 nA, the standards used were natural minerals). The thermo gravimetric analysis was performed in air on 9.62 mg of sample, using a Seiko SSC/5200 instrument, operating at 10 °C/min heating rate, from RT to 900 °C.

The resulting chemical formula was $K_{8.46}(Al_{8.35}Si_{27.53})O_{72} \bullet 17.91H_2O$, with an Si:Al ratio of 3.29. The cell parameters determined at RT were: a =18.3367(1) and c = 7.5176(1)Å.

2.1 Data collection

The temperature-resolved XRPD experiment was performed at the GILDA beam line at the European Synchrotron Radiation Facilities (Grenoble, France). The powder sample was loaded and packed in a 0.3 mm quartz capillary and heated in-situ from RT up to 814 °C by means of a gas blowing system. The heating rate was 5 °C/min. The capillary sample was mounted on a standard goniometric head and spun during data collection in

parallel beam Debye–Scherrer geometry with a monochromatized wavelength of 0.6530 Å. The powder diffraction patterns were collected every 25 °C, on an image plate detector MAR345 positioned at 352 mm from the sample. LaB_6 was used as a standard to calibrate wavelength, sample to detector distance, and tilting angle of the detector. Al_2O_3 thermal expansion was used for temperature calibration. A total of 45 two-dimensional diffraction images were collected and were integrated using Fit2D software [22].

To study the re-hydration process, an XRPD pattern was collected on a small quantity of zeolite L previously heated at 250 °C and left in air for about two months. This pattern was collected at the Centro Interdipartimentale Grandi Strumenti (CIGS) of the University of Modena and Reggio Emilia, using a Panalytical X'Pert PRO diffractometer (θ/θ geometry, CuKα radiation) equipped with an X-celerator detector. A parabolic X-ray mirror was mounted on the incident beam to focus the beam on the sample. The powder was loaded in a glass capillary and spun under the X-ray beam. Data were collected in the 2θ range 3-120° with steps of 0.02° and at 900s per step speed.

2.2 Structural refinement

Structural refinements were performed by full profile Rietveld analysis in the *P/6mmm* space group, using the GSAS package [23] with EXPGUI inter-face [24] and starting from atomic coordinates reported for perlialite [19]. Since no evidence of symmetry change was found from the analysis of the powder patterns, the *P6/mmm* space group was used in all the structure refinements.

A total of 20 patterns were fitted out of the 45 available, selected between RT and 707 °C. Notwithstanding the zeolite maintains a good crystallinity up to 814 °C the diffraction data quality did not allow satisfactory structure refinement above 707 °C and only unit cell parameters were refined. The extracted Bragg peak profiles were modeled by a pseudo-Voight function with two refined coefficients (one Gaussian and one Lorentian term, Gw

and Ly in GSAS terminology) and a 0.01% cut-off of the peak intensity. Due to high diffuse air scattering, the background was partially subtracted and then empirically fitted using a Chebyschev polynomial with 12 variable coefficients. The 2Θ-zero shift was preliminarily refined for all the collected patterns and then fixed at the mean value of the data set, since the variations were very low. The scale factor was allowed to vary for all histograms. In the final cycles, the refined structural parameters for each data histogram were the following: fractional coordinates for all atoms, occupancy factors for extra framework cations and water oxygen atoms, and thermal isotropic displacement factors. H-atoms were not considered during the structure refinement due to their low scattering factors. Soft constraints were applied to the T-O bond distances and were gradually released after the initial stages of refinement. The thermal displacement parameters were constrained in the following way: the same value for all the tetrahedral atoms, a second value for all the framework oxygen atoms, and a third value for the water molecules. The thermal parameters of K sites were free of constraints. Occupancy factors and isotropic thermal displacement factors were varied in alternate refinement cycles. The Rietveld refinements of the powder patterns converged successfully up to 707 °C.

The pattern of the re-hydrated phase was refined starting from the structural model obtained from the data collected at RT, by adopting the above described refinement strategy, except for the number of instrumental background coefficients (25 instead of 12).

The refined cell parameters are reported in Table 1 for each temperature value. Table 2 summarizes the refinement details of four selected patterns, collected at RT, 101 °C, 244 °C, and 707 °C. The refined atomic coordinates, occupancy factors, and thermal parameters for the corresponding structures at these temperatures are reported in Table 3 and the bond distances in Table 4. Figure 2 shows the observed and calculated profiles and the difference curves for the selected patterns.

3. Results

In the investigated temperature range, the cell parameter variations - although very small - are rather discontinuous (Table 1). In the initial heating stage (below 101 °C) zeolite L is essentially rigid, the *a* parameter decreasing and the *c* parameter increasing by less than 0.1% (Figure 3). Between 101º and 244 °C, *a* increases by 0.33 %, *c* decreases by 0.2% and the cell volume undergoes the largest increment observed in the whole investigated T range, i.e. 0.44%. Above 244 °C, the variation trend of *a* and *c* parameters inverts and the V-T curve flattens, though displaying a further slight cell volume increase. The total variations of the *a*, *c*, and *V* parameters are 0.2%, 0.3% and 0.7% , respectively. Zeolite L is stable up to 814 °C and no structural breakdown is observed.

3.1 Framework

Zeolite L framework contains only two independent tetrahedral sites: T1, in the cancrinite cage and T2, shared between the cancrinite cage and the D6R (Figure 1b). The framework structure determined at RT fully agrees with that reported by Barrer and Villiger for their sample[10] (labeled BV below). However, the preference of Al atoms for the T1 site (Table 4), suggested by Newsam [20] on the basis of the bond lengths determined by neutron powder diffraction, was not observed in our study, considering the same T-O bond distances.

During dehydration we observed the following modifications in the zeolite L framework:

i) the main 12MR channel, parallel to the *c* axis, becomes more circular upon heating, as a consequence of the increase and decrease in O1-O2-O1 and O2-O1-O2 angles, respectively (Figures 1a and 4a). The free diameters [9] of the 12MR (O1-O1 and O2-O2) change from 7.2 Å and 7.6 Å at RT, to 7.5 and 7.7 Å at 707 °C, respectively (Figure 4b);

ii) the 8MR channel, parallel to the *c* axis, becomes more circular as a consequence of the decrease and increase of free diameters O1-O1 and O5-O5, respectively (Figures 1a and 5);

iii) during water release, between 101º and 244 °C, the 8MR apertures surrounding the main 12MR channel become more circular, with a decrease in the free diameter O1-O1 (corresponding to the *c* axis trend) and an increase in the O6-O6 one. In contrast, after complete dehydration, above 244 °C, the trend inverts and the rings become more elliptic (Figures 1b and 6);

iv) the T2-O6-T2 angle of the D6R decreases constantly upon heating (Figures 1b and 7) *via* tetrahedral rotation. Also the O4-O4 distance (Figure 8), which can be assumed as the D6R thickness, tends to decrease (even if not in a monotonic way). Moreover, the O3-O5-O3 and O5-O3-O5 angles (Figures 1a and 9) increase and decrease respectively, becoming more similar to each other and hence reducing the di-trigonal distortion of the 6-membered ring.

3.2 Extraframework sites

In the sample at RT, no cations are found at the center of the D6R, in contrast with that reported in [10]. The occupancy factors (Table 3) and the coordination distances (Table 4) of the other cation sites (here labeled KB, KC and KD in Table 3) agree well with the results of the original structural resolution . The slight discrepancies can be explained by the different cation content in BV (6 K and 3 Na a.f.u) and in the present sample (8.46 K a.f.u).

Upon heating, KD slightly shifts from its original position (Table 3) and the potassium distribution on KC and KD sites undergoes a slight reassessment (Figure 10). The KB site maintains the same occupancy factor in all the studied T range, while the occupancy of KD and KC sites decreases and increases, respectively, indicating a partial migration of

potassium from the main channel to the inner KC site. This migration - induced by the necessity of KD to restore its coordination requirements after the loss of the previously coordinated water molecules - ends when the KC site is full. The further decrease in the occupancy of KD - between 244º and 707 °C - can be ascribed to the presence of some water in KD, which is lost above 244 °C.

The main T-induced variations in the bond distances between extraframework cations and framework oxygen atoms (Table 4) are summarized as follows:

-KB-O3 distance increases as a consequence of the 6-ring deformation;

-KC-O5 distance increases, related to the increase of the O5-O5 diameter of the 8MR perpendicular to the *c* axis;

- KD-O4 and KD-O6 bonds shorten during water loss (100-244 °C). This induces a shift of O6 inside the main 12MR channel and a decrease in the T2-O6-T2 angle (Figure 1b). Moreover the O4-O4 distance decreases (Figure 8) determining a decrease in the D6R thickness.

The present zeolite L sample contains at RT 18 water molecules, distributed over five partially occupied sites (labeled WF,WH,WI, WJ, WK in Table 3). They were located in the main channel, but with slightly different coordinates relative to BV. Figure 11 shows the clusters of water molecules and cation-water layers, which develop along the *c* axis. This hydrogen-bonds system is similar to that observed by Lee at al. in their Rb-GaSi L sample [16].

In Figures 12 a and b the variations of the water site occupancy factors and the total number of water molecules in the unit cell are shown as a function of temperature. Most of the water molecules are released above 101 °C, and at 244 °C the zeolite is completely dehydrated. In particular:

- water WI – the most occupied site and the only water molecule bonded to potassium KD –is the last to be completely removed;

- water WF – initially not bonded either to the framework or to the cations – upon heating moves closer to KD and, as a consequence, it is one of the last water molecules to be released ;

- water WH - initially coordinated to the oxygen atom O1 - drifts away during dehydration (Table 4), hence allowing the relaxation of the 12MR aperture along the O1-O1 direction (Figure 4b);

- water WJ, on the contrary, moves closer to the framework oxygen O2 (Table 4) and its release is slower compared to WH. This could explain the almost constant value of the O2-O2 diameter of the 12MR aperture (Figure 4b);

- water WK - bonded only to other water sites - is the freest water molecule and its release begins already at 65 °C.

The total number of water molecules - as calculated from the refined occupancies of all W sites (Table 3 and Figure 12b) - agrees well with the results of the thermal analyses (Figure 13). On the contrary, the temperature corresponding to complete water loss shown by the DTG curve (about 230 °C) is slightly lower than that of the in-situ XRPD experiment (244 °C). This effect can be reasonably explained by the different experimental set up adopted in the two measurements (powdered sample in a small platinum boat in the TG analysis and in a glass capillary in the XRPD experiment).

3.3 Rehydration process

The rehydration of zeolite L was investigated collecting at RT the diffraction pattern of a previously dehydrated sample, subsequently exposed to air for about two months. The structural features of the rehydrated phase can be summarized as follows:

- the cell parameters are almost perfectly recovered (Table 1 and Figure 3);
- the original framework structure of the hydrated phase is almost completely regained (Figures 4-9, 14) although a slight hysteresis is observed;

- potassium cations regain the original distribution on KC and KD (Figure 10);
- WF and WJ sites do not return exactly to the original positions and, more importantly, the original water content is not completely regained (upon rehydration only 16.7 water molecules are found instead of the original 18). In particular, compared to the original zeolite L, the WK site is empty, WF and WI and WJ show a lower occupancy, while WH is slightly more occupied (Figure 12 a,b).

4. Discussion and conclusions

On the basis of the results reported above, the thermal behavior of zeolite L can be summarized as three different steps, corresponding to the following temperature ranges**:**

1. below 100 °C: the structure is essentially unmodified. The cell parameters do not change, dehydration is very limited and involves only the WK and WI site (whose occupancy factors start to decrease), and potassium starts to move from the KD to KC site. This last structural change could be induced by the initial removal and successive complete loss of the WI water molecule, initially coordinated to the KD site;
2. between 101 and 244 °C: complete dehydration of zeolite L occurs, although without inducing notable structural deformations. The 6-membered rings become less ditrigonal and the 12MR apertures become more circular. These last deformations allow easier water diffusion and release and induce an increase of the *a* cell parameter. Moreover, the 8MR channel aperture perpendicular to the *c* axis also becomes more circular. The *a* axis increase is accompanied by a *c* parameter decrease, related to the more circular shape assumed by the 8MR windows which surround the 12MR channel. The driving force of this contraction can be recognized in the attraction of KD to O4. Overall, a small, even if rapid, cell volume increase is observed. The shift of potassium from KD toward KC continues up to 200 °C;

3. above 244 °C: zeolite L is completely dehydrated. After complete water release, the *a* and *c* cell parameters invert their trends and undergo a decrease and increase of about 0.03 Å, respectively. As a whole a steady volume increase is observed (Table 1 and Figure 3). The relaxation of the framework along *c* could be favored by the loss of the WH and WJ water molecules, originally bonded to O1 and O2, and reflected in an increase in the cancrinite cage thickness (see T2-T2 distances in Figure 14).

As reported in the introduction, the structure of potassium zeolite L dehydrated in vacuum at 400 °C was studied by neutron powder diffraction [19], obtaining results rather different from those obtained in the present study. In particular, upon dehydration, the following unit cell parameter variations were observed: +0.4%, -0.8% and -0.03% for *a*, *c* and *V*, respectively. If these data are compared with those obtained for the present sample heated at 422 °C (+0.3%, -0.1% and +0.5%) it is noted that the limited *c* contraction in the present sample is reflected in an overall volume increase. This different behavior can be explained by the following factors which differentiate the two dehydration experiments:

- Newsam's sample ($K_9Al_9Si_{27}O_{72} \cdot 17\ H_2O$) is richer in Al and K and poorer in water compared to the present sample. Moreover the structure refinement showed that potassium is distributed over a different number of extraframework sites;

-the experiment performed by Newsam was conducted with a different kinetics, heating the sample in vacuum very slowly (in several hours) compared to the conditions of our experiment (5 °/min) and maintaining it in vacuum at 400 °C for 16 hours.

The second factor seems to be the crucial one. In fact, as already observed in literature [25], the kinetic conditions play a primary role in the dehydration process of zeolites. In particular, the different kinetics induces a different evolution of the extraframework system (both water molecules and extraframework cations) with a consequent influence on the deformation of the framework.

In general, after Cruciani [5], we can describe the thermal behavior of zeolites on the basis of the following different structural changes: i) cell volume contraction due to the removal of water; ii) displacive or reconstructive phase transformations; iii) negative thermal expansion (NTE); iv) structural collapse; and v) structural breakdown. Several factors have been suggested that might control thermal behavior: i) Si/Al ratio (thermal stability increases with the Si/Al ratio); ii) the ionic potential and size of exchangeable cations and their number (zeolites containing monovalent cations are more stable than those containing divalent ones); iii) the coordination of bare cations after water expulsion; and iv) the framework topology.

The same author also discusses the behavior of pure silica zeolites, suggesting that in these phases an expansion of the unit cell is expected upon heating. Actually, while most zeolites exhibit a so-called negative thermal expansion (see[5] for a review), a positive one is observed in a number of neutral siliceous zeolites, like CIT-5, AlPO4-31 and the one-dimensional 12MR system ITQ-4 [26]. In these materials expansion is mainly realized along the direction of the main large 12- or 14-ring channel, as observed in the zeolite L investigated here.

In his review of the factors influencing zeolite thermal stability, Cruciani[5] also defines a Stability Index (SI) scale (from 1 to 5 in value) on the basis of the collapse temperature. The SI of zeolite L is equal to 5. This result is particular noteworthy due to the rather low Si/Al ratio (3.3) of this zeolite, which would suggest a lower thermal stability.

Finally, the inverse relationship between thermal stability and ionic potential of the extraframework ions - potassium in the present sample - was confirmed by the results of this study. Usually, in zeolites, most of the extraframework cations are coordinated by water molecules. Upon dehydration these cations move closer to the framework to form new bonds. This can induce strains on the framework, resulting in a structural deformation

or even bond breaking. Zeolite L represents an exception, because only one of the three cation sites (KD) is bonded to a water molecule, while the coordination spheres of the other cations are formed only by framework oxygen atoms. Moreover, among the five water molecules, only two are at coordination distance from the framework oxygen atoms, while the others are only involved in water-water hydrogen bonds. These structural features explain why the dehydration process does not induce substantial structural modifications in the host framework and why zeolite L even undergoes a small unit cell volume increase upon heating.

In this work it was determined that, overall, zeolite L has a very high thermal stability and maintains a good crystallinity up to 814 °C. Following Baur [27], this framework can be classified as inflexible upon changes in both physical and chemical conditions. Currently, literature reports the ability of LTL topology to host different framework and extraframework cationic forms and a variable number of water molecules without substantial structural modifications[4,10] . In particular, concerning the response to heating under the experimental conditions adopted in the present study, it is noteworthy that zeolite L undergoes a slight thermal expansion, which is a very unusual behavior for an alumino-silicate microporous material.

Acknowledgements

The authors thank Satoshi Ohtake for technical support in zeolite synthesis, Raul Carampin of the CNR (Padua) for the EMPA analysis, and Simona Bigi for the TG analyses. This work was supported by the Italian MIUR (PRIN2008 and PRIN2009). The Italian beamline (GILDA) at the European Synchrotron Radiation Facility is acknowledged for allocating beamtime and for technical support during the experiments.

Figure captions

Figure 1. Projection along the *c* axis (a) and view from the inside of the 12MR channel (b) of potassium zeolite L at room temperature. Light grey: water sites; dark grey: K sites.

Figure 2. Observed (crossed line) and calculated (continuous line) diffraction patterns and final difference curve from Rietveld refinements of zeolite L at RT, 101º, 244º, and 707°C.

Figure 3. Normalized unit cell parameters *vs*. temperature. The grating symbols correspond to the rehydrated phase.

Figure 4. Temperature-induced shape change of the12MR delimiting the main channel parallel to *c* axis: a) O2-O1-O2 and O1-O2-O1 angles; b) O1-O1 and O2-O2 free diameters (calculated assuming an oxygen radius of 1.35 Å) [9]. The grating symbols correspond to the rehydrated phase.

Figure 5. Temperature-induced shape change of the 8MR delimiting the corresponding channel parallel to *c* axis: O1-O1 and O5-O5 free diameters (calculated assuming an oxygen radius of 1.35 Å) [9]. The grating symbols correspond to the rehydrated phase.

Figure 6. Temperature-induced shape change of the 8MR windows surrounding the 12MR channel: O1-O1 and O6-O6 free diameters (calculated assuming an oxygen radius of 1.35 Å) [9]. The grating symbols correspond to the rehydrated phase.

Figure 7. Variation in T-O-T angles *vs*. temperature. The grating symbols correspond to the rehydrated phase.

Figure 8. Thickness of the D6R (O4-O4 distance) as a function of temperature.

Figure 9. Variation of the O3-O5-O3 and O5-O3-O5 angles of the 6-rings of the D6R *vs*. temperature. The grating symbols correspond to the rehydrated phase.

Figure 10. Plot of K sites occupancy factors *vs*. temperature. The grating symbols correspond to the rehydrated phase.

Figure 11. Sequence of water clusters and cation-water layers running along the *c* axis inside the 12MR channel. The distances W-W between 2.65 and 2.89 (Å) are drawn. Light grey: water sites; dark grey: KD site.

Figure 12. Occupancy factors of water sites in zeolite L (a) and total water content per unit cell (b) *vs*. temperature. The grating symbols correspond to the rehydrated phase.

Figure 13. TG (continuous line) and DTG (dashed line) curves of zeolite L.

Figure 14. Variation of cancrinite cage thickness (T2-T2) *vs*. temperature. The grating symbols correspond to the rehydrated phase.

Table captions

Table 1. Unit cell parameters of zeolite L as a function of temperature.

Table 2. Experimental and refinement parameters for zeolite L at RT, 101º, 244º, and 707°C.

Table 3. Atomic coordinates, occupancy factors and thermal parameters for the structures at RT, 101º, 244º, and 707°C.

Table 4. Framework and extraframework bond distances less than 3.2 Å. The too short distances can be justified by the not simultaneously presence of the involved atoms, due to their partial occupancy factors.

References

[1] A. Alberti, and G. Vezzalini, In: Proceedings of the 6th International Zeolite Conference. Reno. Eds. D.Olson and A.Bisio. Butterworth, Guildford, U.K. (1984) 834-841.

[2] K. Ståhl, Materials Science Forum 166-169 (1994) 571-576.

[3] G. Artioli, In: Microscopic properties and processes in minerals, K. Wright, R. Catlow eds., NATO Science Series, Series C, 543 (1999) 177-187. Kluwer, Dordrecht.

[4] D.L. Bish, and Carey J. W. (2001) In: Natural zeolites: occurrence, properties, applications, D.L. Bish, D.W. Ming eds., Reviews in Mineralogy and Geochemistry, MSA, 45, 403-452.

[5] G**.** Cruciani J. Phys. Chem. Solids 67 (2006) 1973–1994.

[6] G. Calzaferri, S. Huber, H. Maas, C. Minkowski, Angew. Chem., Int. Ed. 42 (2003) 3732–3758.

[7] D. Brühwiler, G. Calzaferri, T. Torres, J.H. Ramm, N. Gartmann, L.Q. Dieu, I. López-Duarte, M. Martínez Díaz, J. Mater. Chem. 19 (2009) 8040–8067.

[8] Y. Wang, H. Li, Y. Feng, H. Zhang, G. Calzaferri, T. Ren, Angew. Chem., Int. Ed. 49 (2010) 1434–1438.

[9] Ch. Baerlocher, L.B. McCusker, D.H. Olson, Atlas ofZeolite Framework Types, 6th ed., Elsevier, Amsterdam (2007).

[10] R.M. Barrer, and H. Z. Villiger, Z. Kristallogr. 128 (1969) 352-370.

[11] M. Pauchard, A. Devaux, G. Calzaferri, Chem. Eur. J. 6 (2000) 3456–3470.

[12] L. Gigli, G. Agostini, R. Arletti, E. Fois, C. Lamberti, G. Tabacchi, S. Quartieri, G. Vezzalini, Proc. European Mineralogical Conference 2012 (2012) 24.

[13] D.W. Breck and E.M. Flanigen. In Molecular Sieves, R.M. Barrer, Ed; Society of Chemical Industry, London (1968) 47-61

[14] Ch. Baerlocher and R.M. Barrer, Z. Kristallogr. 136 (1972) 245-254.

[15] J.M. Newsam, Mater. Res. Bull. 21 (1986) 661-672.

[16] Y. Lee, S. J. Kim, D.C. Ahn and N.S. Shin, Chem. Mater. 19 (2007) 2277-2282.

[17] N. Venkatathri, Indian J. Chem. Sect A. 41 (2002) 2223-2230.

[18] D.W. Breck and G.W. Skeels, U.S. Patent 4,503,023 (1985).

[19] G. Artioli and Å Kvick, Eur. J. Mineral. 2 (1990) 749-759.

[20] J.M. Newsam, J.Phys.Chem. 93 (1989) 7689-7694.

[21] J.P. Verduijn, U.S. Patent 5, 242, 675 (1993).

[22] A. P. Hammersley, S. O. Svensson, M. Hanfland, A. N. Fitch, D. Häusermann, High Pressure Research 14 (1996) 235-248.

[23] A.C. Larson, R.B. Von Dreele, General Structure Analysis System "GSAS", Los Alamos National Laboratory Report LAUR 86-748, (1994).

[24] B.H. Toby, J. Appl. Crystallogr. 34 (2001) 210–213.

[25] R. Arletti, E. Mazzucato, G. Vezzalini, Amer. Mineral. 91 (2006) 628-634.

[26] P. Lightfoot, D. A. Woodcock, M.J. Maple, L. A. Villaescusa, P. A. Wright, J. Mater. Chem. 11 (2001) 212 .

[27] W. H. Baur, J. Solid State Chem. 97 (1992) 243-247.

Figure 1a

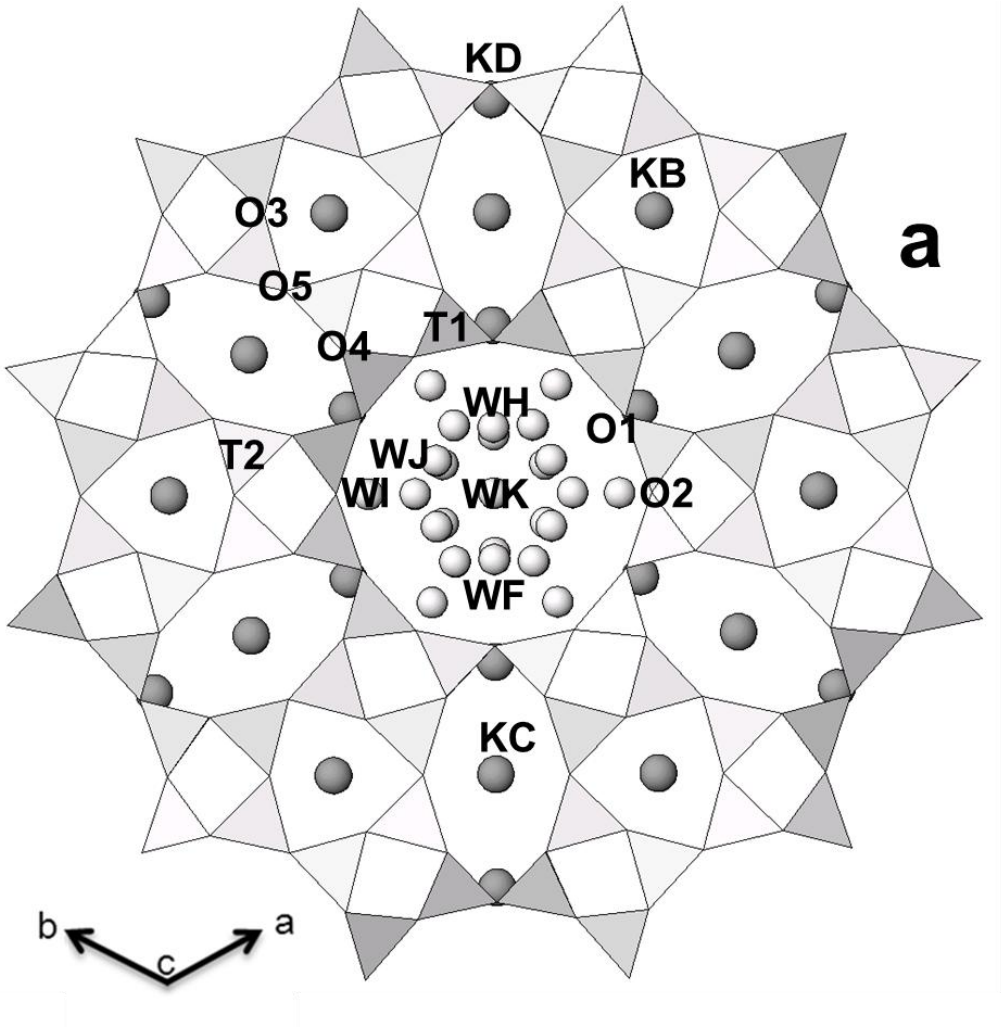

Figure 1b

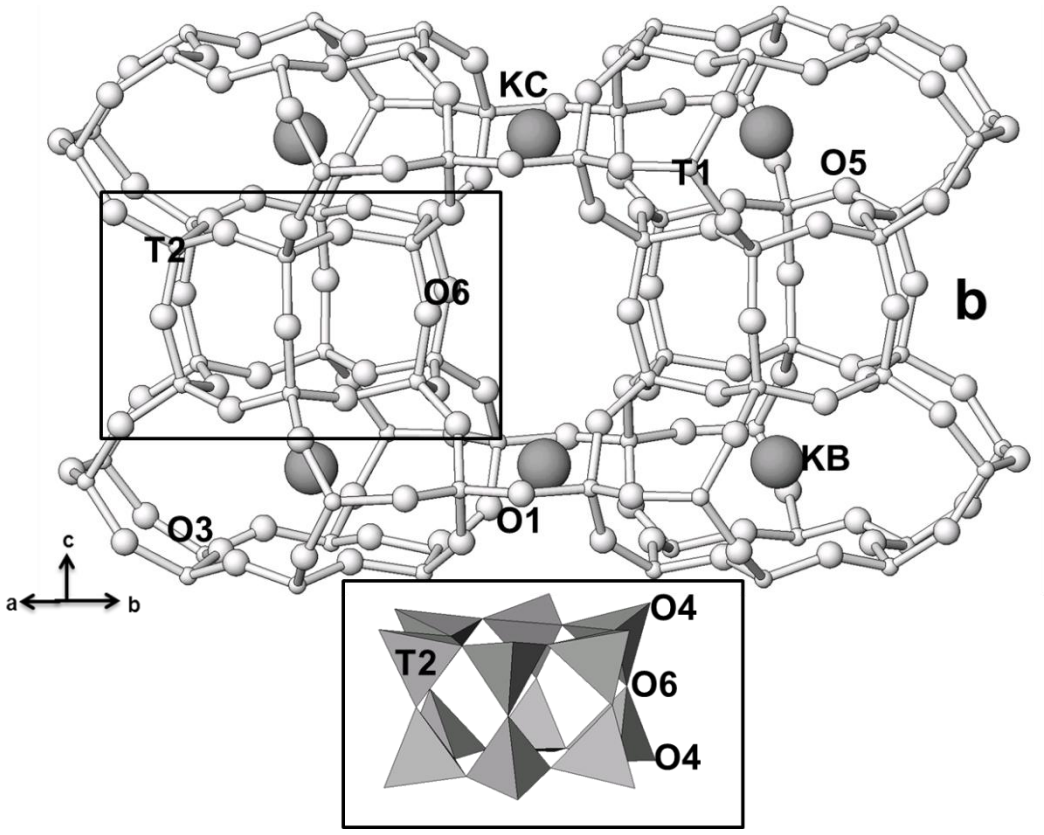

Figure 2

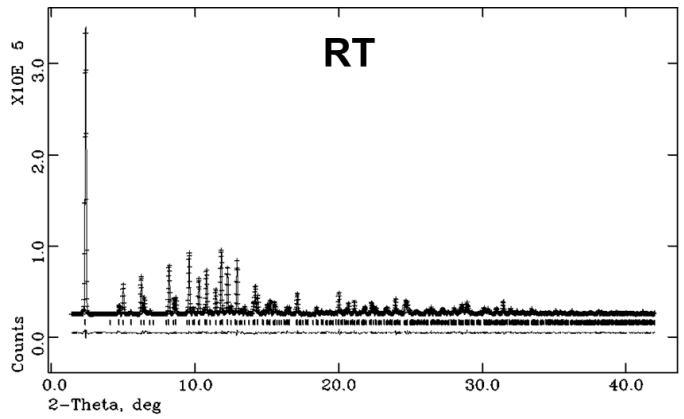
RT
X10E 5
3.0
2.0
1.0
0.0
Counts
0.0
10.0
20.0
30.0
40.0
2-Theta, deg

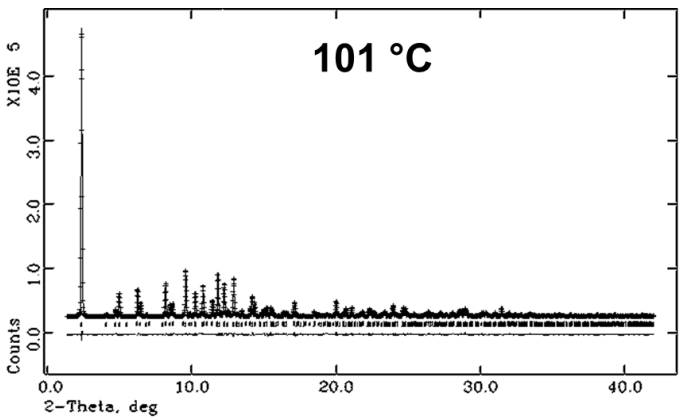
101 °C
X10E 5
4.0
3.0
2.0
1.0
0.0
Counts
0.0
10.0
20.0
30.0
40.0
2-Theta, deg

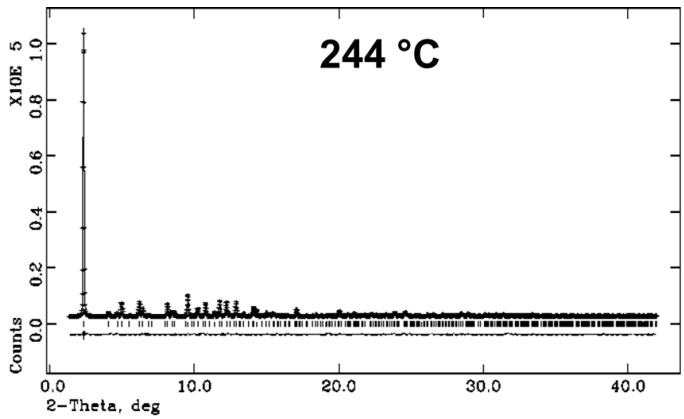
244 °C
X10E 5
1.0
0.8
0.6
0.4
0.2
0.0
Counts
0.0
10.0
20.0
30.0
40.0
2-Theta, deg

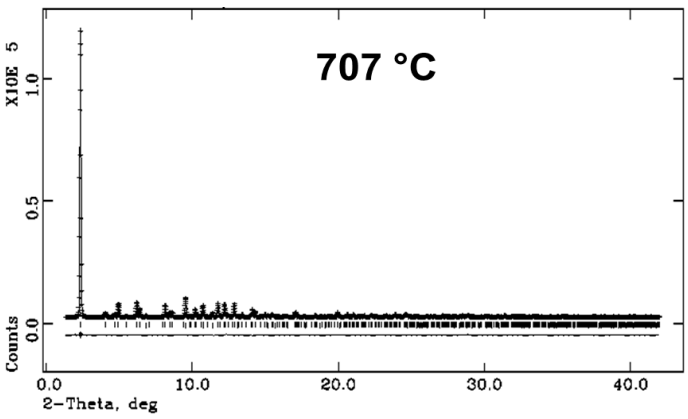
707 °C
X10E 5
1.0
0.5
0.0
Counts
0.0
10.0
20.0
30.0
40.0
2-Theta, deg

Figure 3

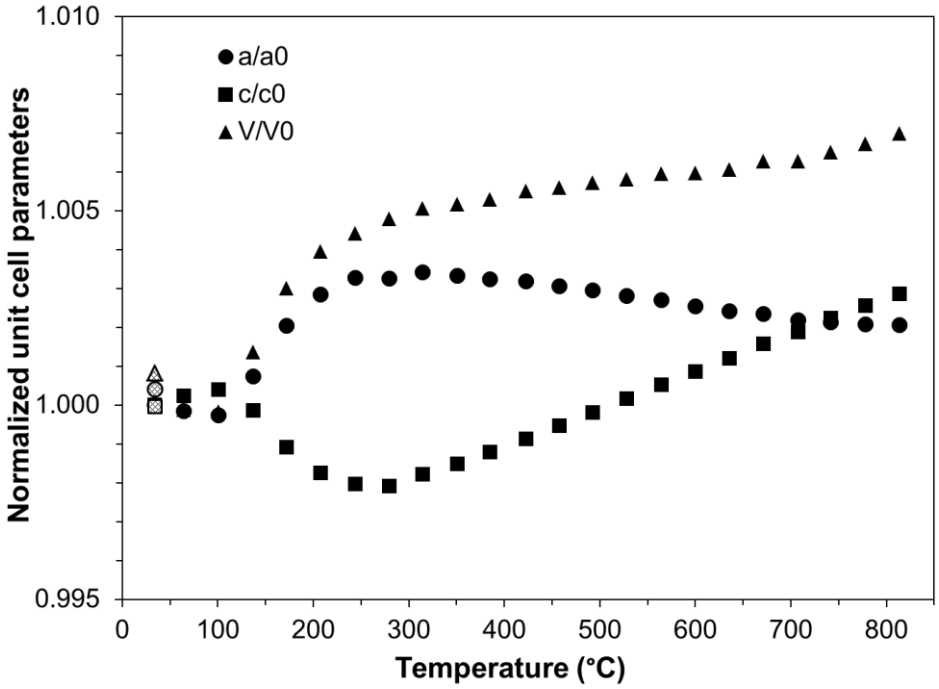
a/a0
c/c0
V/V0
Normalized unit cell parameters
1.010
1.005
1.000
0.995
0
100
200
300
400
500
600
700
800
Temperature (°C)

Figure 4a,b

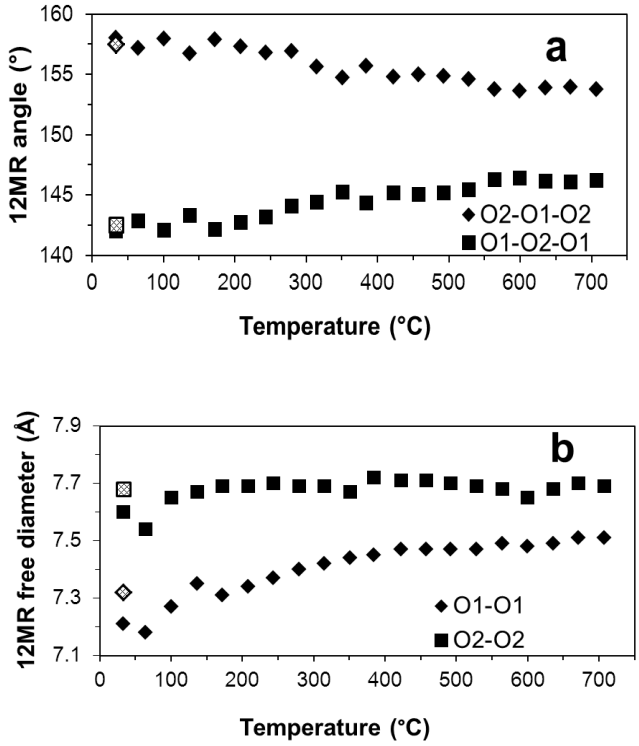
a
12MR angle (°)
160
155
150
145
140
0
100
200
300
400
500
600
700
Temperature (°C)
O2-O1-O2
O1-O2-O1
b
12MR free diameter (Å)
7.9
7.7
7.5
7.3
7.1
0
100
200
300
400
500
600
700
Temperature (°C)
O1-O1
O2-O2

Figure 5

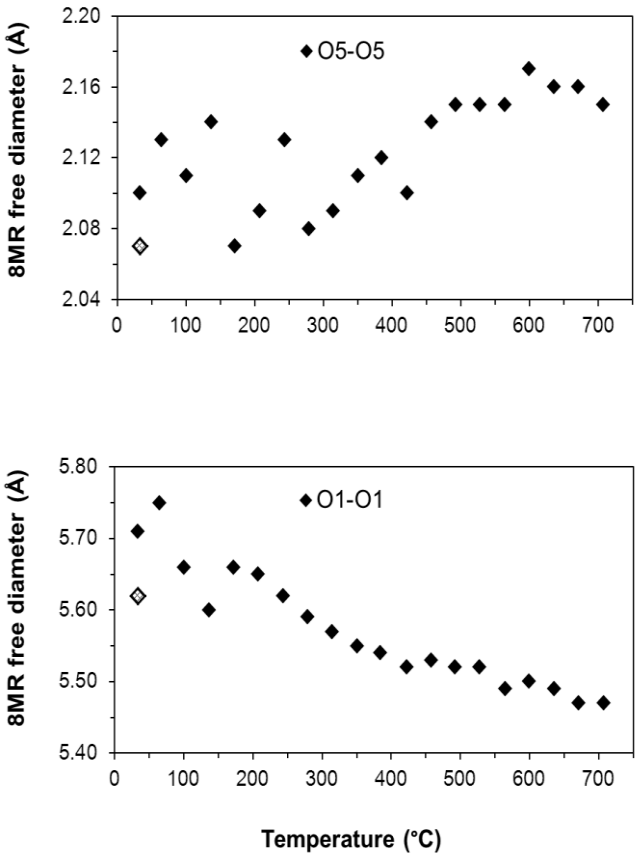
8MR free diameter (Å)
O5-O5
2.20
2.16
2.12
2.08
2.04
0
100
200
300
400
500
600
700
8MR free diameter (Å)
O1-O1
5.80
5.70
5.60
5.50
5.40
0
100
200
300
400
500
600
700
Temperature (°C)

Figure 6

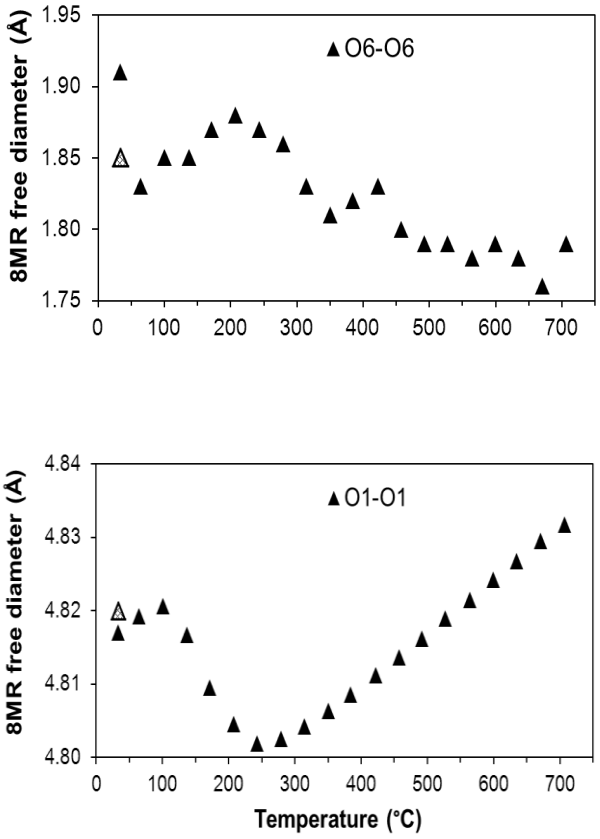
8MR free diameter (Å)
1.95
1.90
1.85
1.80
1.75
O6-O6
0
100
200
300
400
500
600
700
8MR free diameter (Å)
4.84
4.83
4.82
4.81
4.80
O1-O1
0
100
200
300
400
500
600
700
Temperature (°C)

Figure 7

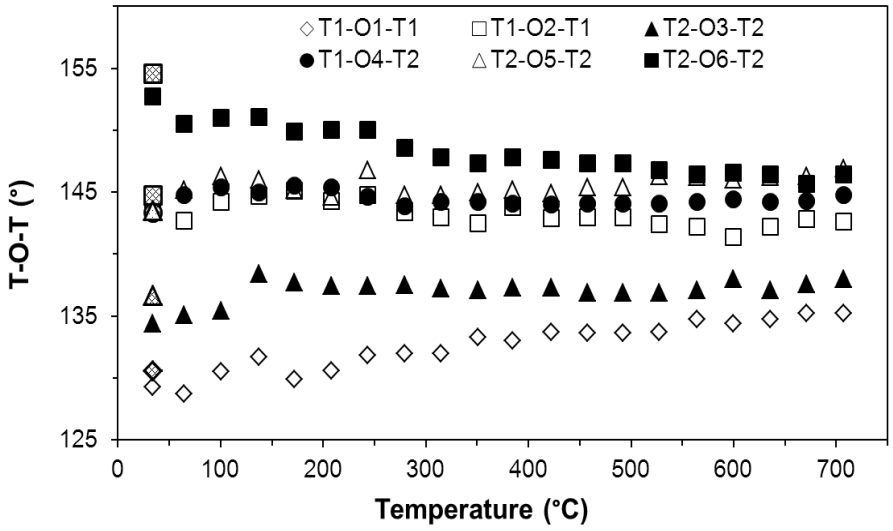
◇T1-O1-T1
□T1-O2-T1
▲T2-O3-T2
●T1-O4-T2
△T2-O5-T2
■T2-O6-T2
155
145
135
125
T-O-T (°)
0
100
200
300
400
500
600
700
Temperature (°C)

Figure 8

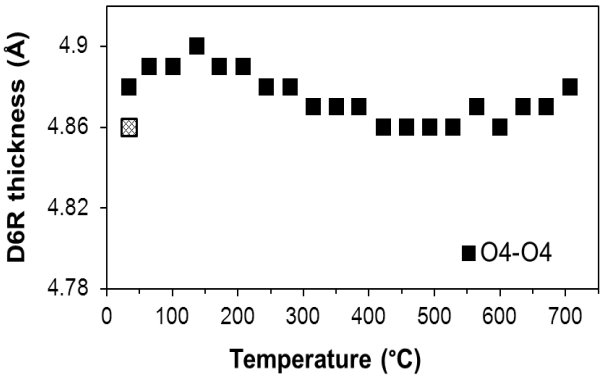
D6R thickness (Å)
4.9
4.86
4.82
4.78
0
100
200
300
400
500
600
700
Temperature (°C)
O4-O4

Figure 9

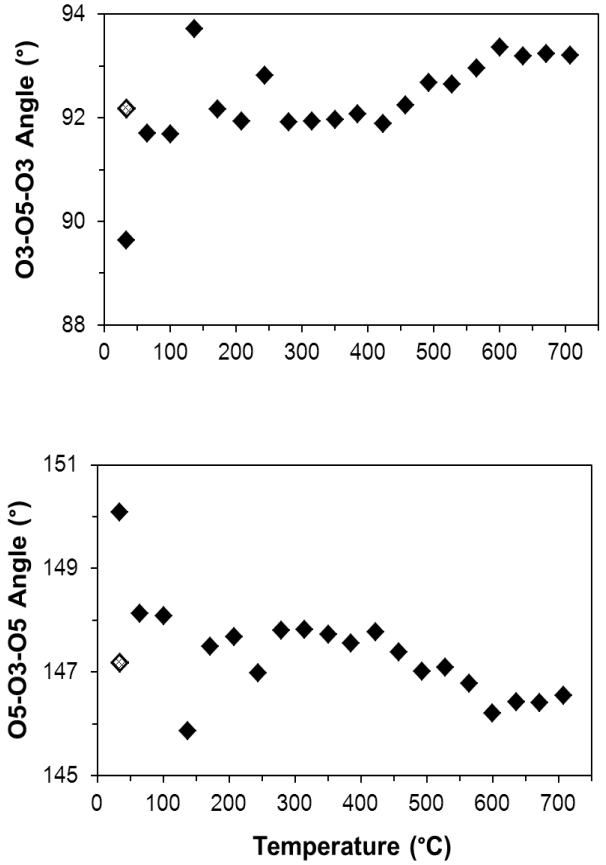
O3-O5-O3 Angle (°)
94
92
90
88
0
100
200
300
400
500
600
700
O5-O3-O5 Angle (°)
151
149
147
145
0
100
200
300
400
500
600
700
Temperature (°C)

Figure 10

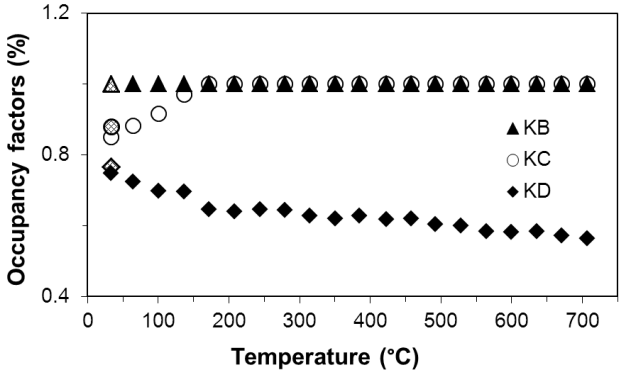
1.2
0.8
0.4
Occupancy factors (%)
0
100
200
300
400
500
600
700
Temperature (°C)
KB
KC
KD

Figure 11

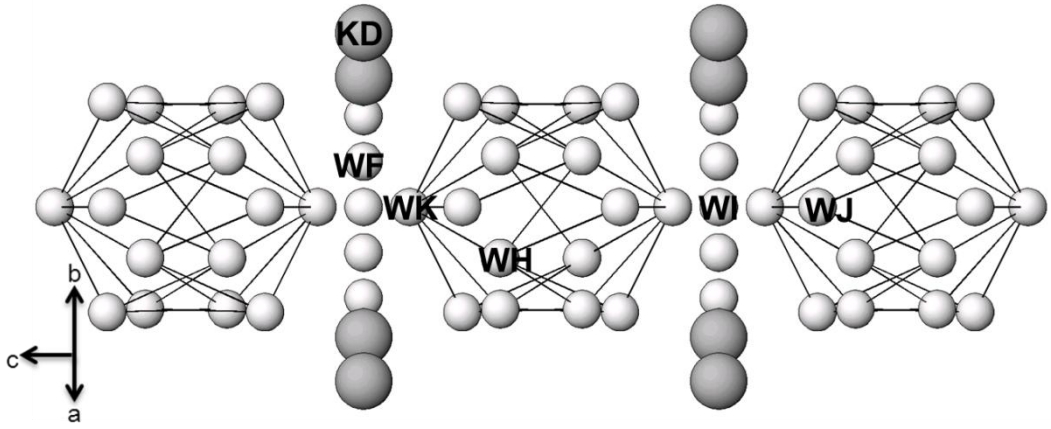

Figure 12 a,b

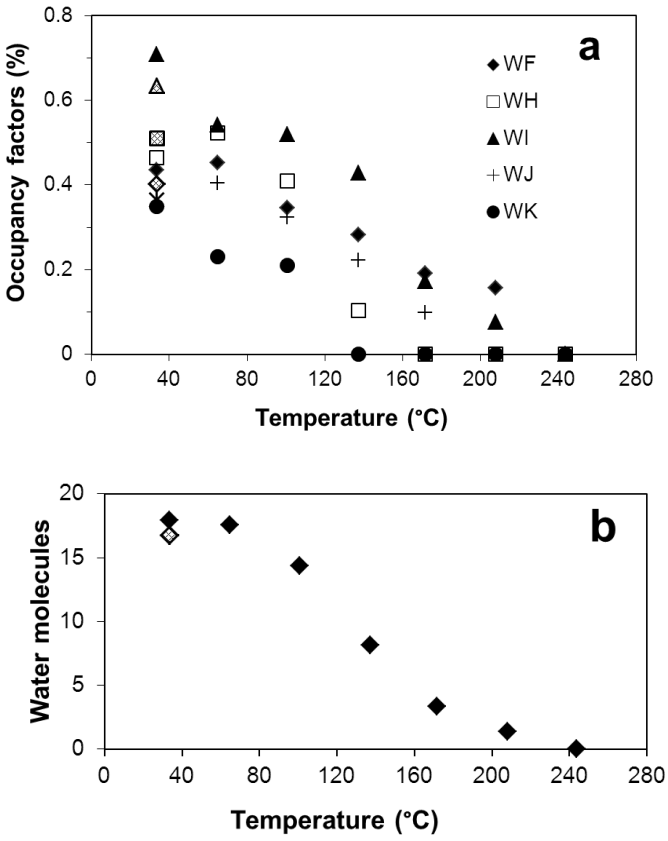
a
Occupancy factors (%)
0.8
0.6
0.4
0.2
0
0
40
80
120
160
200
240
280
Temperature (°C)
WF
WH
WI
WJ
WK
b
Water molecules
20
15
10
5
0
0
40
80
120
160
200
240
280
Temperature (°C)

Figure 13

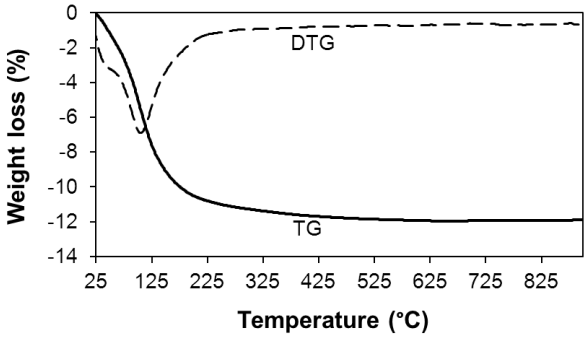
0
-2
-4
-6
-8
-10
-12
-14
Weight loss (%)
DTG
TG
25
125
225
325
425
525
625
725
825
Temperature (°C)

Figure 14

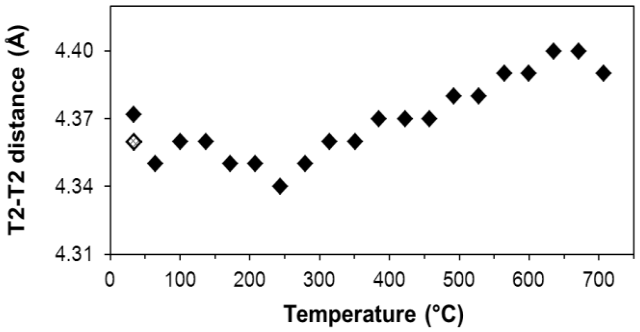
T2-T2 distance (Å)
4.40
4.37
4.34
4.31
0
100
200
300
400
500
600
700
Temperature (°C)

Table 1

Table 1. Unit cell parameters of zeolite L as a function of temperature.

T(°C)	a (Å)	c (Å)	V(Å^3)
RT	18.3367(1)	7.5176(1)	2189.06(4)
65	18.3338(2)	7.5194(1)	2188.78(5)
101	18.3320(1)	7.5206(1)	2188.66(4)
137	18.3504(2)	7.5166(1)	2192.04(5)
172	18.3741(2)	7.5095(1)	2195.62(5)
208	18.3889(2)	7.5045(1)	2197.71(5)
244	18.3968(2)	7.5023(1)	2198.72(4)
280	18.3964(1)	7.5019(1)	2199.53(5)
315	18.3994(2)	7.5042(1)	2200.11(7)
351	18.3978(2)	7.5062(1)	2200.35(5)
385	18.3962(2)	7.5085(1)	2200.62(5)
422	18.3950(2)	7.5111(1)	2201.10(5)
458	18.3929(2)	7.5136(1)	2201.30(5)
492	18.3909(2)	7.5162(1)	2201.58(5)
528	18.3883(2)	7.5188(1)	2201.76(5)
565	18.3864(2)	7.5215(1)	2202.06(5)
600	18.3833(2)	7.5241(1)	2202.11(5)
635	18.3810(2)	7.5267(1)	2202.31(5)
671	18.3796(2)	7.5295(1)	2202.79(5)
707	18.3769(1)	7.5317(1)	2202.79(4)
742	18.3757(1)	7.5344(1)	2203.29(4)
778	18.3747(1)	7.5368(1)	2203.75(4)
814	18.3745(1)	7.5391(1)	2204.36(4)
RT(REV)	18.3445(2)	7.5174(1)	2190.85(5)

Table 2

Table 2. Experimental and refinement parameters for zeolite L at RT, 101º, 244º, and 707 °C.

T (°C)	RT	101	244	707
Space Group	P6/m m m	P6/m m m	P6/m m m	P6/m m m
a (Å)	18.3367(2)	18.3320(1)	18.3968(2)	18.3769(1)
c (Å)	7.5176(1)	7.5205(1)	7.5019(1)	7.5317(1)
V ($Å^3$)	2189.06(5)	2188.66(4)	2198.72(4)	2202.79(4)
R_p (%)	1.4	1.3	1.1	1.1
R_{wp} (%)	1.9	1.9	1.6	1.6
R F2 (%)**	8	7.46	6.75	9.7
X^2	10.5	10.3	0.80	0.78
No. of variables	55	55	42	42
No. of observations	2889	2889	2889	2889
No. of reflections	673	673	673	673

Table 3

Table 3. Atomic coordinates, occupancy factors and thermal parameters for the structures at RT, 101º, 244º, and 707 °C.

Atom	x/a	y/b	z/c	Occ.	Uiso
		RT			
T1	0.0939(1)	0.3566(2)	0.5	1	0.0136(5)
T2	0.1646(2)	0.4978(1)	0.2093(2)	1	0.0136(5)
O1	0	0.2694(6)	0.5	1	0.0159(9)
O2	0.1616(2)	0.3233(5)	0.5	1	0.0159(9)
O3	0.2671(2)	0.5342(4)	0.2534(8)	1	0.0159(9)
O4	0.1019(3)	0.4127(3)	0.3241(5)	1	0.0159(9)
O5	0.4245(2)	0.8490(4)	0.2645(9)	1	0.0159(9)
O6	0.1452(4)	0.4762(4)	0	1	0.0159(9)
KB	0.3333	0.6666	0.5	1	0.022(7)
KC	0.5	0	0.5	0.850(5)	0.018(2)
KD	0.2989(3)	0	0	0.753(4)	0.084(2)
WF	0.111(1)	0	0	0.434(7)	0.138(8)
WH	0.1186(7)	0	0.384(1)	0.465(5)	0.138(8)
WI	0.2576(9)	0.1288(5)	0	0.70(1)	0.138(8)
WJ	0.165(1)	0.0830(7)	0.281(2)	0.399(5)	0.138(8)
WK	0	0	0.142(7)	0.35(1)	0.138(8)
		101 °C			
T1	0.0949(2)	0.3575(2)	0.5	1	0.015(6)
T2	0.1646(2)	0.4974(1)	0.2110(2)	1	0.015(6)
O1	0	0.2732(6	0.5	1	0.016(1)
O2	0.1630(2)	0.3261(5)	0.5	1	0.016(1)
O3	0.2655(2)	0.531114)	0.2586(9)	1	0.016(1)
O4	0.1026(3)	0.4145(3)	0.3233(5)	1	0.016(1)
O5	0.4241(2)	0.8483(4)	0.268(1)	1	0.016(1)
O6	0.1432(4)	0.4747(4)	0	1	0.016(1)
KB	0.3333	0.6666	0.5	1	0.039(2)
KC	0.5	0	0.5	0.916(6)	0.030(2)
KD	0.3002(4)	0	0	0.699(4)	0.094(4)
WF	0.118(1)	0	0	0.345(7)	0.141(1)
WH	0.1139(7)	0	0.357(1)	0.409(4)	0.141(1)
WI	0.255(1)	0.1276(6)	0	0.52(1)	0.141(1)
WJ	0.210(1)	0.1095(7)	0.204(4)	0.323(6)	0.141(1)
WK	0	0	0.094(1)		
		244 °C			
T1	0.0942(1)	0.3575(1)	0.5	1	0.021(5)
T2	0.1659(2)	0.4981(1)	0.2105(2)	1	0.021(5)
O1	0	0.2740(5)	0.5	1	0.027(1)
O2	0.1633(2)	0.3266(5)	0.5	1	0.027(1)
O3	0.2646(2)	0.5293(4)	0.2542(8)	1	0.027(1)
O4	0.1022(2)	0.4140(2)	0.3253(5)	1	0.027(1)
O5	0.4241(1)	0.8483(3)	0.2648(9)	1	0.027(1)
O6	0.1434(3)	0.4746(3)	0	1	0.027(1)
KB	0.3333	0.6666	0.5	1	0.035(2)
KC	0.5	0	0.5	1	0.050(2)
KD	0.3129(3)	0	0	0.644(3)	0.065(2)
		707 °C			
T1	0.0951(2)	0.3591(2)	0.5	1	0.035(5)
T2	0.1652(2)	0.4983(2)	0.2078(2)	1	0.035(5)
O1	0	0.2775(6)	0.5	1	0.044(1)
O2	0.1628(3)	0.3256(5)	0.5	1	0.044(1)
O3	0.2646(2)	0.5292(4)	0.2516(8)	1	0.044(1)
O4	0.1026(3)	0.4139(3)	0.3240(4)	1	0.044(1)
O5	0.4237(2)	0.8475(4)	0.2620(9)	1	0.044(1)
O6	0.1408(4)	0.4707(4)	0	1	0.044(1)
KB	0.3333	0.6666	0.5	1	0.085(3)
KC	0.5	0	0.5	1	0.094(2)
KD	0.3095(4)	0	0	0.573(3)	0.093(4)

Table 4

Table 4. Framework and extraframework bond distances less than 3.2Å. The excessively short distances are justified by the partial occupancy of the sites involved.

	RT	101 °C	244 °C	707 °C
T1-O1	1.654(5)	1.655(5)	1.648(5)	1.641(4)
O2	1.627(4)	1.616(4)	1.634(4)	1.636(3)
O4 [X2]	1.636(4)	1.639(4)	1.633(3)	1.629(3)
average	1.638	1.637	1.637	1.634
T2-O3	1.681(4)	1.669(4)	1.645(4)	1.653(4)
O4	1.647(5)	1.624(5)	1.636(5)	1.645(5)
O5	1.617(3)	1.624(3)	1.628(2)	1.616(3)
O6	1.616(2)	1.634(2)	1.633(2)	1.636(2)
average	1.640	1.638	1.636	1.638
KB-O3 [x6]	2.809(6)	2.830(6)	2.859(6)	2.879(6)
KC-O5 [x4]	2.985(6)	2.976(6)	2.994(6)	3.013(6)
KD-O4 [x4]	3.145(2)	3.151(2)	3.078(5)	3.094(4)
O6 [x2]	3.005(6)	2.948(6)	2.822(7)	2.800(5)
WI [x2]	2.819(4)	2.842(4)		
WF-WF[x2]	2.06(2)	2.19(2)		
WH [x2]	2.891(1)	2.688(1)		
WI [x2]	2.53(1)	2.53(1)		
WJ[x4]	2.502(2)	2.42(1)		
WK [x2]	2.32 (2)	2.30(2)		
WH-O1	2.93(1)	3.08(1)		
WF[x2]	2.891(1)	2.688 (1)		
WH[x2]	2.16(1)	2.08(1)		
WH	1.71(2)	2.10(3)		
WH[x2]	2.75(2)	2.96 (2)		
WJ[x2]	1.540(6)	1.540(6)		
WJ[x2]	2.83(1)	2.201(8)		
WK	2.83(1)	2.89(1)		
WI-KD [x2]	2.819(4)	2.842(4)		
WF[x2]	2.53(1)	2.53(1)		
WJ[x2]	2.562(7)	1.693(7)		
WJ-O2	2.98(1)	2.87(2)		
WF[x2]	2.51(2)	2.38(2)		
WH[x2]	1.56(1)	2.18(2)		
WH[x2]	2.84(2)			
WI	2.562(7)	1.693(7)		
WJ[x2]	2.66(1)	3.12(4)		
WK	2.86(1)			
WK-WF[x6]	2.31(2)	2.29(2)		
WH[x6]	2.84(2)	2.91(6)		
WJ[x6]	2.86(1)			
WK	2.10(9)	1.37(2)		